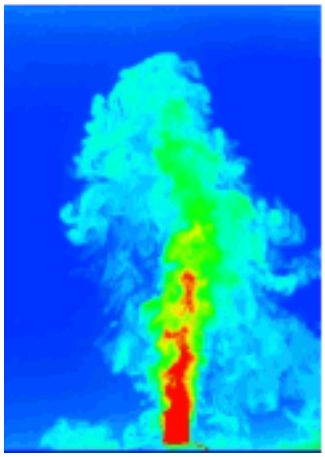

Journal of Turbulence
Publication details, including instructions for authors and subscription information:
http://www.informaworld.com/smpp/title~content=t713665472

Particle dispersion and wall-dependent turbulent flow scales: implications for local equilibrium models

Cristian Marchioli [a]; Maurizio Picciotto [a]; Alfredo Soldati [a]
[a] Dipartimento di Energetica e Macchine, Centro Interdipartimentale di Fluidodinamica e Idraulica, Università degli Studi di Udine, Via delle Scienze 208. Udine, 33100. Italy

To link to this article: DOI: 10.1080/14685240600925171
URL: http://dx.doi.org/10.1080/14685240600925171

Journal of Turbulence
Volume 7, No. 60, 2006

Particle dispersion and wall-dependent turbulent flow scales: implications for local equilibrium models

CRISTIAN MARCHIOLI, MAURIZIO PICCIOTTO and ALFREDO SOLDATI*

Centro Interdipartimentale di Fluidodinamica e Idraulica, Dipartimento di Energetica e Macchine, Università degli Studi di Udine, Via delle Scienze 208, 33100 Udine, Italy

Theoretical models for particle dispersion in turbulent wall layers are based on closure assumptions for particle-turbulence correlations which strongly depend on the wall-normal coordinate. This paper presents new data for the near-wall dispersion of inertial particles in fully developed turbulent channel flow, obtained using direct numerical simulation (DNS) with a one-way point-particle approach. The link between wall-dependent flow time scales and particle time scales is discussed addressing further the issue of using integral flow time scales to parametrize particle behavior. This is fundamental to validate closure relations in theoretical local-equilibrium models for particle dispersion in wall-bounded flows, where the reduction of the fluid velocity fluctuation in the wall-normal direction is not accompanied by an equivalent reduction of the particle velocity fluctuation.

1. Introduction

Particle dispersion in turbulent flows is a highly non-uniform process which is dominated by quasi-deterministic coherent structures. Inertial particles respond selectively to these structures giving rise to macroscopic phenomena such as local segregation or preferential concentration. In the specific case of boundary layers, particle response to turbulence leads to irreversible accumulation at the wall, large concentration gradients and high particle deposition rates [1–3].

To elucidate the physics of the dispersion process, the above-mentioned features of near-wall particle behavior are put in evidence in figure 1. This figure has been obtained using raw data and concentration statistics extracted from our DNS database and shows the instantaneous position of particles dispersed in fully developed channel flow (figure 1(a), (c)), together with the corresponding number density distribution, $n_p(z^+)$, along the wall-normal direction, z^+ (figure 1(b), (d)). Particle number density distribution is calculated as in Soldati [4] and the superscript $+$ is used to indicate non-dimensional variables in wall units†. Two different time instants are considered: $t^+ = 0$ (figure 1(a), (b)), when particles are introduced at random positions in the domain assuming an initial uniform distribution, and $t^+ = 1125$ (figure 1(c), (d)), when particles are not homogeneously distributed and tend to form clusters. From these

*Corresponding author. Also affiliated with Department of Fluid Mechanics, CISM, 33100 Udine, Italy. E-mail: soldati@uniud.it.

† In reporting our results, we will present all quantities in wall units (or inner scaling) obtained using the fluid kinematic viscosity, ν, and the shear velocity, u_τ. The shear velocity is $u_\tau = (\tau_w/\rho)^{1/2}$, where τ_w is the mean shear stress at the wall and ρ is fluid density.

Journal of Turbulence
ISSN: 1468-5248 (online only)
http://www.tandf.co.uk/journals
DOI: 10.1080/14685240600925171

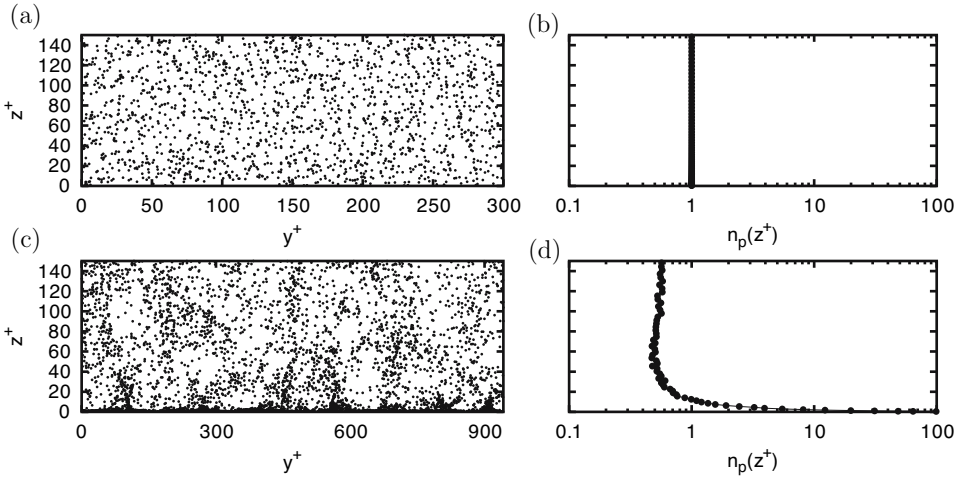

Figure 1. Cross-sectional view of particle instantaneous distribution (a, c) and corresponding number density distribution, n_p, as a function of the wall-normal coordinate z^+ (b, d). Snapshots are taken at different simulation times: $t^+ = 0$ (a, b) and $t^+ = 1125$ (c, d). Mean flow is directed toward the reader in figures (a) and (c).

clusters, particles are continuously transported toward the wall, accumulating into specific 'reservoirs' where concentration build-up occurs [3, 5]. Particles tend to stay for long times (from hundred to thousand time wall units [6]) in these reservoirs so that eventually particle concentration increases near the wall: at the time of figure 1(d), the particle number density distribution, $n_p(z^+)$, has developed a maximum well into the viscous sublayer ($0 < z^+ < 5$).

The integral value of $n_p(z^+)$ in the viscous sublayer (computed as $n_p^{\mathrm{int}}(t^+) = \int_0^5 n_p(z^+, t^+)\,\mathrm{d}z^+$ and normalized to the total number of particles in the channel) is shown in figure 2 as a function of time for particles with different inertia. The Stokes number, St, is used to characterize particle inertia. In wall turbulence, the Stokes number may be defined as τ_p/τ_f, where τ_p is the particle response time and τ_f is an appropriate turbulence time scale.

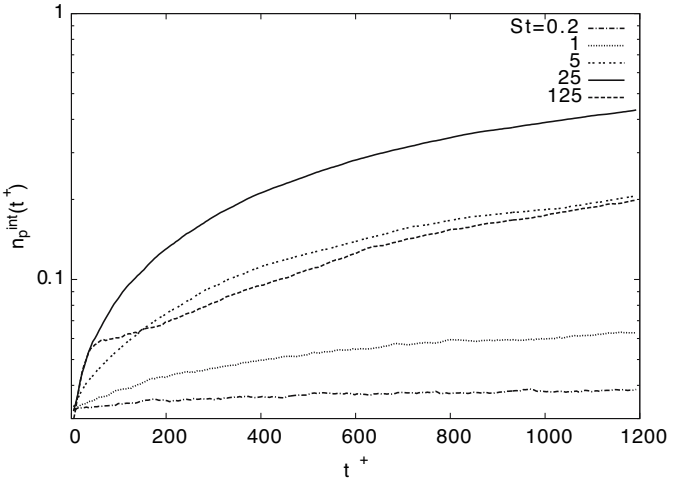

Figure 2. Time evolution of particle number density in the viscous sublayer, n_p^{int}.

The particle response time is defined here as $\tau_p = \rho_p d_p^2/18\rho\nu$, where ρ_p and d_p are particle density and diameter respectively, while ρ is the fluid density. The turbulence time scale in wall units is defined as $\tau_f = \nu/u_\tau^2$.

From figure 2, it is apparent that particle number density profiles tend toward a statistically steady state; the rate of convergence is very slow and depends on particle inertia. Also, depending on inertia is the wall concentration value reached by the particles. As suggested by previous analyses [2, 5], the largest concentration at the wall occurs when the flow structures time scale and the particle time scale are comparable. In our flow configuration, high-Stokes-number particles ($St = 125$) respond only to the lowest fraction of the spectrum of turbulence and their motion lacks coherent clustering mechanisms. At the other extreme, low-Stokes-number particles ($St = 0.2$) act almost as flow tracers. Maximum concentration at the wall is found for the intermediate-Stokes-number particles ($St = 25$), indicating that the time scale of the coherent vortical structures which actually cause the preferential concentration is appropriate for scaling [5].

However, these structures vary from flow to flow. For instance, in channel flow (as in the present case) particle distribution will be determined by the Stokes number based on the large-vortices turnover time, whereas the Stokes number based on the Kolmogorov time scale might be more relevant in homogeneous turbulence, where the small-scale dissipative eddies are responsible for the non-randomness of particle distribution. Whichever is the case, none of the state-of-the-art physical models for particle dispersion in turbulent flows incorporates the information required to predict such structural behavior. In this paper, we will focus our attention on models which assume a proportionality between the particle and the fluid Reynolds stresses (local equilibrium assumption) [7–10]. To reproduce experimental or numerical data of particle dispersion in complex turbulent flows, these models use simple closure equations for particle–turbulence correlations. Predictions strongly depend on the closure assumptions used to compute the statistical features of the fluid turbulent motions (particularly those seen by the dispersed phase) and appear not adequate in the near-wall region [11, 12]. Problems arise when there is a significant particle drift due to turbulence inhomogeneities; particles entrained by vortical structures in one region of the flow acquire sufficient momentum to move into regions with different turbulence characteristics while retaining a memory of their earlier motion. This memory effect complicates the attempt to model the near-wall particle behavior through simple correlations.

In this paper, we study the near-wall behavior of inertial particles in fully developed turbulent channel flow, using DNS with a one-way point-particle approach. Specific objectives of the study are: (i) to investigate the relationship between flow time scales and particle time scales in wall-bounded turbulence and (ii) to identify suitable flow time scales for parametrization of near-wall particle behavior through theoretical models. To these objectives, new statistics have been selectively extracted from our DNS dataset, gathered in the frame of a more general work on the numerical simulation of turbulent dispersed flows.

The outline of the paper is as follows. First, we describe the formulation of the problem and the numerical method; then, we present results on the Lagrangian integral time scales characterizing channel flow. In the last part of the paper, implications of using these time scales for modeling particle near-wall behavior are discussed.

2. Numerical methodology

The numerical experiments are performed using a pseudo-spectral solver of the fluid balance equations, described in previous papers [13, 14], coupled with a Lagrangian particle tracking routine.

The flow into which particles are introduced is a pressure-driven turbulent channel flow of air, assumed incompressible and Newtonian. In the present study, we consider air with density $\rho = 1.3$ kg m^{-3} and kinematic viscosity $\nu = 15.7 \times 10^{-6}$m^{2}s^{-1}. The reference geometry consists of two infinite flat parallel walls; the origin of the coordinate system is located at the center of the channel and the x-, y- and z-axes point in the streamwise, spanwise and wall-normal directions, respectively. Periodic boundary conditions are imposed on the fluid velocity field both in streamwise and in spanwise directions, and no-slip boundary conditions are imposed at the walls. As mentioned, all variables made dimensionless using ν and the wall-shear velocity u_τ are characterized by the superscript $+$. Calculations are performed on a computational domain of $1885 \times 942 \times 300$ wall units in x, y and z discretized with $128 \times 128 \times 129$ nodes; the grid spacing in the streamwise and spanwise directions is $\Delta x^+ = 14.7$ and $\Delta y^+ = 7.35$ respectively. The spacing of collocation points in the wall-normal direction ranges from $\Delta z^+_{\min} = 0.045$ at the wall to $\Delta z^+_{\max} = 3.687$ at the channel centerline. Domain size and grid resolution appear sufficient to describe the significant length scales in the flow [15–17]. The shear Reynolds number is $Re_\tau = u_\tau h/\nu = 150$, where h is the channel half-height.

The Lagrangian particle tracking routine coupled with the DNS code was developed to calculate particle trajectories in the flow field. The code interpolates the fluid velocity at discrete grid nodes onto the particle position by means of sixth-order Lagrangian polynomials: the interpolation scheme is slightly less accurate than that of spectral direct summation and shows good agreement with a hybrid scheme which uses sixth-order Lagrangian polynomials in the streamwise and spanwise directions and Chebychev summation in the wall-normal direction. Once the fluid velocity at the particle position is known, the equations of particle motion are advanced in time by means of a fourth-order Runge–Kutta scheme. Particles are non-interacting, pointwise, rigid, spheres initially released at random locations within the computational box. Particle density is $\rho_p = 10^3$ kg m^{-3}, large compared to fluid density. The particle concentration is assumed to be small enough to neglect the influence of the particles on the fluid and inter-particle interactions (hydrodynamic interactions and collisions). A particle is elastically reflected away from the wall when its center is less than a distance equal to one-particle radius from the wall. The particle momentum balance equation as discussed by Maxey and Riley [18] was simplified according to previous works [19–21] neglecting lift, virtual mass, pressure gradient force and Basset force. We did not consider gravity effects either. With these simplifications, the only forces considered are inertia and drag and the following Lagrangian equation for the particle velocity is obtained [18]:

$$\frac{\mathrm{d}\mathbf{u}_p}{\mathrm{d}t} = -\frac{3}{4}\frac{C_D}{d_p}\left(\frac{\rho}{\rho_p}\right)|\mathbf{u}_p - \mathbf{u}|(\mathbf{u}_p - \mathbf{u}), \tag{1}$$

where $\mathbf{u}_p$ and $\mathbf{u}$ are the particle and fluid velocity vectors respectively, d_p is the particle diameter and C_D is the drag coefficient computed according to the nonlinear model proposed by Schiller and Naumann [22]:

$$C_D = \frac{24}{Re_p}\left(1 + 0.15Re_p^{0.687}\right), \tag{2}$$

where Re_p is the particle Reynolds number ($Re_p = d_p|\mathbf{u}_p - \mathbf{u}|/\nu$). The correction for C_D is necessary because Re_p does not necessarily remain small, in particular for depositing particles. Faxen correction to the viscous drag has been neglected. Simulations were run by tracking sets of 10^5 particles, each set being characterized by a different value of the Stokes number (from $St = 0.2$ to $St = 125$). Particle parameters are given in table 1. The derivation of equation (1) assumes that the particle is small compared to the length scales in the undisturbed flow, the strain rate is small and the particle Reynolds number is small. The first assumption, in particular, imposes that (i) the grid cell has to be significantly larger than the particles since

Table 1. Particle parameters.

d_p (μm)	$d_p^+ = d_p v/u_\tau$	τ_p (ms)	$St = \tau_p/\tau_f$
9.1	0.068	0.2254	0.2
20.3	0.152	1.122	1
45.6	0.342	5.660	5
102	0.764	28.32	25
228	1.71	141.5	125

the velocity used to calculate the forces acting on the particles is the velocity of the continuous phase at the particle center (point-particle approach).

On the other hand, (ii) the accuracy required by DNS imposes a grid cell smaller than the smaller fluid scale of the flow, namely the Kolmogorov length scale in the present case. The non-dimensional Kolmogorov length scale, η_K^+, for our channel flow has an average value of 2 wall units, its local value ranging from 1.6 wall units near the wall to 3.6 wall units near the channel centerline. This means that the minimum grid spacing along the wall-normal direction, $\Delta z_{\min}^+$, is roughly 35 times smaller than the local Kolmogorov length scale.

In direct numerical simulations of particle-laden turbulent flows, requirements (i) and (ii) can be satisfied if the particles are much smaller than the Kolmogorov length scale. Strictly speaking, this is not the case for the $St = 125$ particles, which are characterized by a non-dimensional diameter, d_p^+, of 1.71 wall units yielding $d_p^+/\eta_K^+ \simeq O(1)$. Also, these particles touch the wall when their center is at an impact distance of 0.855 wall units from the wall: at this distance, particle dimension is slightly larger than the grid size, which is equal to 0.73 wall units. When doing one-way coupling simulations, however, the surrounding fluid is not being disturbed by the particles, and the only consequence of using a small grid cell is that the particles see a local flow field with smaller scales than the ones that are forcing the actual particles [23]. Depending on the type of particle, this can introduce significant errors in the computation of particle trajectories. For heavy particles in a gas flow, typically, the particle response time can be significantly larger than the Kolmogorov time scale. In the present case, the non-dimensional particle response time, τ_p^+, is given precisely by the Stokes number and is equal to 125 for the larger particles. The non-dimensional average value of the Kolmogorov time scale is $\tau_K^+ = 4$, its local value ranging from 2 time-wall units at the wall to 13 time-wall units at the channel centerline yielding $\tau_p^+/\tau_K^+ \simeq 31$. Thus, the larger particles are driven mostly by the large scales, and we expect the error introduced by a small grid cell not to be large.

We also remark here that, in small Reynolds number wall turbulence and in the case of heavy particles, the flow Reynolds number has little effect on particles. Current simulations at a higher Reynolds number ($Re_\tau = 360$) [12] do not show strong differences; however, effects might become more important if the shear Reynolds number is further increased.

The timestep used was $\mathrm{d}t^+ = 0.045$ and the total simulation time was $t^+ = 1192$ for each particle set. We remark here that this simulation time is not long enough to achieve a statistically steady state for the particle phase. When a statistically steady situation is not yet achieved, a net flux of particles toward the wall is established. In a steady state, the flux of particles toward the wall must be balanced by the flux in the opposite direction returning the particles to the bulk of the flow. However, it is not obvious that a non-trivial statistically steady state can be achieved for all particle sizes. In the case of large particles, whose mean free path is comparable with or larger than the size of near-wall region, a mechanism for such a flux can be provided by elastic wall collision of particles having large wall-normal velocity. In the case of particles with a small mean free path, the interaction with the wall will resemble an

absorbing-wall condition rather than an elastic-bouncing condition [12], and the statistically steady state might be trivial: empty bulk flow and densely populated near-wall region.

3. Particle and flow time scales in turbulent boundary layer

3.1 *Lagrangian integral time scales in channel flow*

In the introduction, we mentioned that the level of non-randomness of the particle spatial distribution is mostly determined by particle selective response to turbulence. However, the flow scales that are dynamically relevant to the phenomena of local accumulation and segregation vary from flow to flow and it is impossible to match systematically the particle Stokes number. For instance, peak preferential concentration of particles in homogeneous isotropic turbulence (HIT) occurs at Stokes numbers of $O(1)$ when the particle time scale, τ_p, is normalized to the Kolmogorov time scale of the flow, τ_η [2, 17, 24]. Thus, the correct scaling for particle response to turbulent eddies in HIT is related to τ_η. This piece of information can be very useful to develop models which must account for the effect produced by the inertial drift of particles in a homogeneous turbulent field. In wall-bounded flows, retrieving a relevant time scale is complicated by the non-homogeneity associated with the direction normal to the wall. Consider for instance figure 3(a), which shows the behavior of the non-dimensional Kolmogorov time scale, τ_η^+, as a function of the non-dimensional distance from the wall, z^+, in the present channel flow configuration. From a minimum value of $\sim$2.6 at the wall, τ_η^+ increases up to a maximum value of $\sim$12.8 at the channel centerline. Figure 3(b) shows the corresponding behavior of the particle relaxation times considered in this study with respect to z^+, when normalized to the Kolmogorov time scale. Let us focus on the intermediate-Stokes-number particles, namely $St = \tau_p/\tau_f = 25$ (black solid line), which undergo maximum wall accumulation [5]. From figure 3(b), we observe that the ratio τ_p/τ_η is $O(10)$ close to the wall and decreases to values slightly larger than 1 at the channel centerline. In the proximity of a wall boundary, the specification of the adequate fluid time scale to characterize particle accumulation is indeed difficult. Most theoretical models [7, 9, 25–27] use an integral time scale, representing the large, energetic turbulent motions responsible for particle drift toward regions of decreasing turbulence intensity. This effect, known as 'turbophoresis' [28], is a manifestation of the skewness in the velocity distribution of the particles and, for large enough inertia,

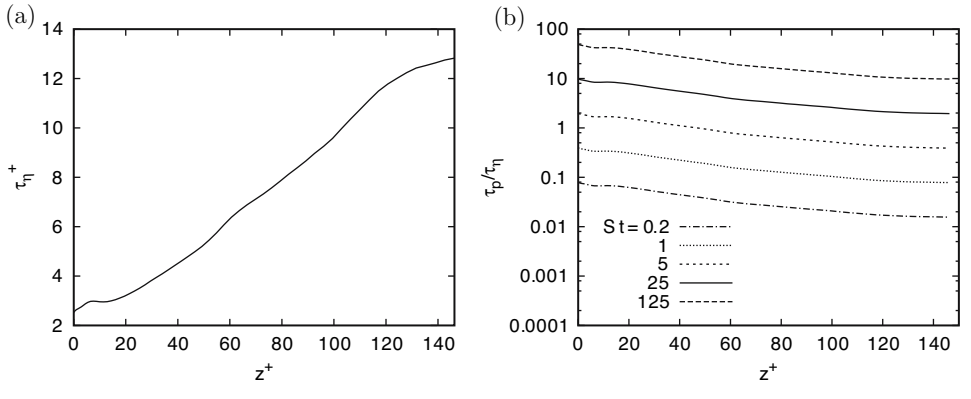

Figure 3. (a) Behavior of the non-dimensional Kolmogorov time scale, τ_η^+, and (b) behavior of the particle-to-Kolmogorov time scale ratio, τ_p/τ_η, as a function of the wall distance, z^+.

it becomes the main mechanism governing particle dynamic behavior. As a matter of fact, turbophoresis is the cause of the macroscopic phenomenon observed in figure 1(c) and (d).

Accurate representation of the turbophoretic effect in the particle momentum equations is difficult because, due to the convective particle drift, the wall-normal component of the mean-square fluctuating velocity of the particles may not relate directly to the wall-normal component of the mean-square fluctuating velocity of the fluid. To overcome this difficulty, models assume local equilibrium between the particle–velocity fluctuation, u'_p, and the fluid-velocity fluctuation, u'_f [7–10]. Under this assumption, the particle-velocity fluctuation is everywhere proportional to the fluid-velocity fluctuation. More precisely, the particle Reynolds stresses, $u'_{p,i}u'_{p,j}$, and the fluid Reynolds stresses , $u'_{f,i}u'_{f,j}$, are assumed proportional according to the following equation:

$$\langle u'_{p,i}u'_{p,j}\rangle_p = \Gamma\ \langle u'_{f,i}u'_{f,j}\rangle_f\ , \tag{3}$$

where the angle brackets indicate ensemble averaging. In principle, the local equilibrium coefficient, Γ, can be a complicated higher-order tensor.

From a practical viewpoint, if one is able to model Γ, then one would have a model for the turbophoretic effect, which could be used (together with a 'particle-drift-velocity' model) to predict particle deposition. Theoretical models use ad hoc modifications of Γ to take into account the different components of the Reynolds stress tensors so that Γ becomes a mix between a scalar and a higher-order tensor. Specifically, the simplest engineering models (see Young and Leeming [7] or Sergeev *et al.* [9] among others) assume:

$$\Gamma = C\frac{1}{1+St_{\mathrm{L}}}, \tag{4}$$

where C is a constant and $St_{\mathrm{L}} = \tau_p/\tau_g$ is the Stokes number based on the local persistence time of the turbulent fluid eddies, τ_g. It is not straightforward to precisely specify such a time scale. One possible choice is to set τ_g equal to some integral time scale of the fluid, which can be either estimated from Eulerian statistics [26, 27] or, as in the present work, computed in a Lagrangian way assuming an exponential decay of the fluid velocity autocorrelation function [7, 10, 25].

Equation (3) can be applied in homogeneous isotropic turbulence, yet it requires careful handling in wall-bounded flows, where St_{L} is not necessarily constant, as demonstrated in figure 4, where the wall-normal behavior of the Lagrangian integral time scale of the fluid,

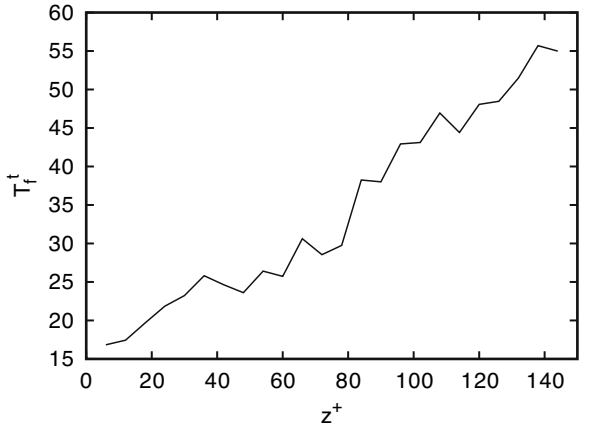

Figure 4. Lagrangian integral time scale of the fluid, T_f^t, as a function of the wall-normal coordinate, z^+.

indicated as T_f^t, is shown. The procedure to compute T_f^t was as follows. First, using a sample of $O(10^5)$ massless fluid tracers released in the domain, in the time interval $\Delta t^+ = 742 \div 1192$ the fluid velocity autocorrelation function was obtained according to the following equation:

$$R_{f,ij}(t + \mathrm{d}t, \mathbf{x}_f(t + \mathrm{d}t)) = \frac{\langle u'_{f,i}(t + \mathrm{d}t, \mathbf{x}_f(t + \mathrm{d}t)) u'_{f,j}(t, \mathbf{x}_f(t)) \rangle_f}{\langle u'_{f,i}(t, \mathbf{x}_f(t)) u'_{f,j}(t, \mathbf{x}_f(t)) \rangle_f}. \tag{5}$$

$R_{f,ij}$ is computed along each fluid tracer path; the subscript f denotes the dependence of $R_{f,ij}$ on the instantaneous position of the fluid tracers, $\mathbf{x}_f(t)$, and the angle brackets $\langle \rangle_f$ indicate ensemble averaging on tracer distribution. In equation (5), the velocity fluctuations were calculated as $u'_{f,i}(t, x_{f,i}(t)) = u_{f,i}(t, x_{f,i}(t)) - \langle u_{f,i}(t, x_{f,i}(t)) \rangle_f$, where the last term is also equal to the space-averaged Eulerian fluid velocity [27]. The Lagrangian integral time scale of the fluid reads as [7, 10, 27]:

$$T_{f,ij}^t = \int_0^\infty R_{f,ij}(t)\, \mathrm{d}t. \tag{6}$$

To compute $T_{f,ij}^t$: (i) we divided the channel height into 50 uniformly spaced bins, (ii) we computed the autocorrelation functions $R_{f,ij}$ over time by recording the initial position of the fluid tracers, (iii) following Simonin *et al.* [27], we computed the integrals for the diagonal elements of $R_{f,ij}$ (namely the correlations $R_{f,11}$, $R_{f,22}$ and $R_{f,33}$). Finally, the resulting values were averaged to obtain T_f^t. As for $R_{f,ij}$, the time span considered for the calculation was Δt^+. For the range of particle time scales considered in the present study, sampling intervals 10% larger/smaller than Δt^+ were sufficient for obtaining fluid Lagrangian integral time scales which were converged, i.e. increases/decreases in the sampling interval did not appreciably change the output of the computation. In contrast, it must be pointed out that the value of T_f^t depends on the number of bins chosen for the calculation.

The value of T_f^t changes significantly with the distance from the wall at which it is computed; in the center of the channel, T_f^t is three times larger than at the wall. Therefore, $St_\mathrm{L} = \tau_p / T_f^t$ must become three times smaller.

Several Eulerian models [27, 29] use closure assumptions based on the statistical characteristics of the fluid turbulent motion viewed by the dispersed phase. According to these models, if the fluid velocity is evaluated along the particle trajectory, then the autocorrelation function for the fluid at the particle position can be calculated as:

$$R_{fp,ij}(t + \mathrm{d}t, \mathbf{x}_p(t + \mathrm{d}t)) = \frac{\langle u'_{f,i}(t + \mathrm{d}t, \mathbf{x}_p(t + \mathrm{d}t)) u'_{f,j}(t, \mathbf{x}_p(t)) \rangle_p}{\langle u'_{f,i}(t, \mathbf{x}_p(t)) u'_{f,j}(t, \mathbf{x}_p(t)) \rangle_p}. \tag{7}$$

The Lagrangian integral time scale of the fluid at the particle position, T_{fp}^t, is then calculated upon substitution of $R_{f,ij}(t + \mathrm{d}t, \mathbf{x}_f(t + \mathrm{d}t))$ with $R_{fp,ij}(t + \mathrm{d}t, \mathbf{x}_p(t + \mathrm{d}t))$ in equation (6). The subscript p denotes the dependence of $R_{fp,ij}$ on the instantaneous particle position, $\mathbf{x}_p(t)$, while the angle brackets $\langle \rangle_p$ indicate ensemble averaging on the particle distribution.

Figure 5 shows the wall-normal behavior of St_L when the particle response time is normalized to either the Lagrangian integral time scale of the fluid ($St_\mathrm{L} = \tau_p / T_f^t$, figure 5(a)) or the Lagrangian integral time scale of the fluid at the position of the particles ($St_\mathrm{L} = \tau_p / T_{fp}^t$, figure 5(b)). All particle sets are considered here. From a qualitative viewpoint, the two plots look similar. In particular, for the $St = 25$ particles (black solid line), we find that St_L is $O(1)$ in the proximity of the wall. This result shows that both the integral time scales are more suitable than the Kolmogorov time scale to model the near-wall particle behavior since they match the scales that are most dynamically relevant to particle dispersion. Thus, T_f^t and T_{fp}^t can be used to parametrize the particle velocity fluctuations starting from the fluid velocity fluctuations, which are assumed known [7].

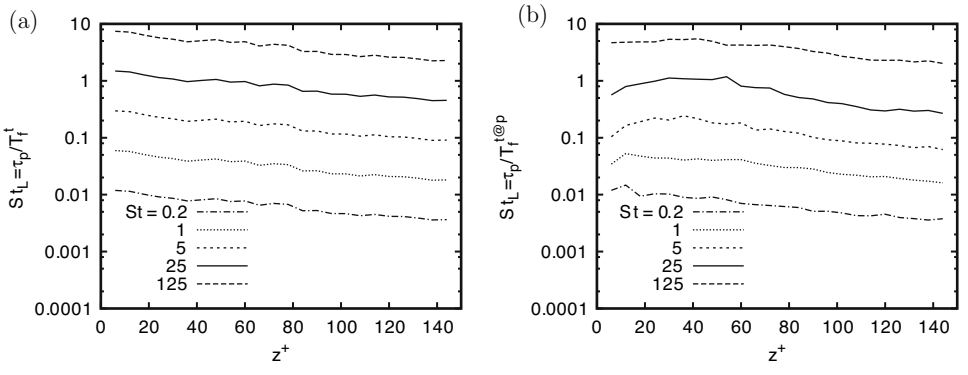

Figure 5. Wall-normal behavior of St_L, defined as the ratio of the particle relaxation time to (a) the Lagrangian integral time scale of the fluid, $St_L = \tau_p / T_f^t$ and to (b) the Lagrangian integral time scale of the fluid at a particle position, $St_L = \tau_p / T_{fp}^t$.

3.2 *Time scaling under local equilibrium assumptions*

As mentioned in section 3.1, local-equilibrium models assume a proportionality between the fluid Reynolds stresses and the particle Reynolds stresses: $\langle u'_{p,i} u'_{p,j} \rangle_p = \Gamma \, \langle u'_{f,i} u'_{f,j} \rangle_f$.

Figure 6 shows the ratio of the particle diagonal Reynolds stresses, $\langle u'_{p,i} u'_{p,i} \rangle_p = \langle u'^2_{p,i} \rangle_p$, to the fluid diagonal Reynolds stresses, $\langle u'_{f,i} u'_{f,i} \rangle_p = \langle u'^2_{f,i} \rangle_f$, as a function of the wall-normal coordinate z^+ for the streamwise (figure 6(a): index $i = 1$) and the wall-normal (figure 6(b): index $i = 3$) directions. This ratio gives the value of Γ extracted from our numerical database. The subscripts and angle brackets for fluid and particles have the same meaning as in equations (6) and (7), respectively. The fluid velocity fluctuations are fully Eulerian (the fluid velocity is not evaluated at particle position) and averaged over a time span equal to Δt^+; the particle velocity fluctuations are computed as $u'_{p,i} = u_{p,i} - \langle u_{p,i} \rangle_p$, $\langle u_{p,i} \rangle_p$ being the velocity ensemble averaged on particle distribution.

For ease of reading, in figure 6 we use a logarithmic scale to amplify the near-wall region. In both directions, the value of Γ is roughly constant and equal to unity except very close to the wall (roughly, $z^+ < 10$ in the streamwise direction and $z^+ < 5$ in the wall-normal direction). In the streamwise direction (figure 6(a)), we find that Γ is $O(1)$ even at the wall for the smaller

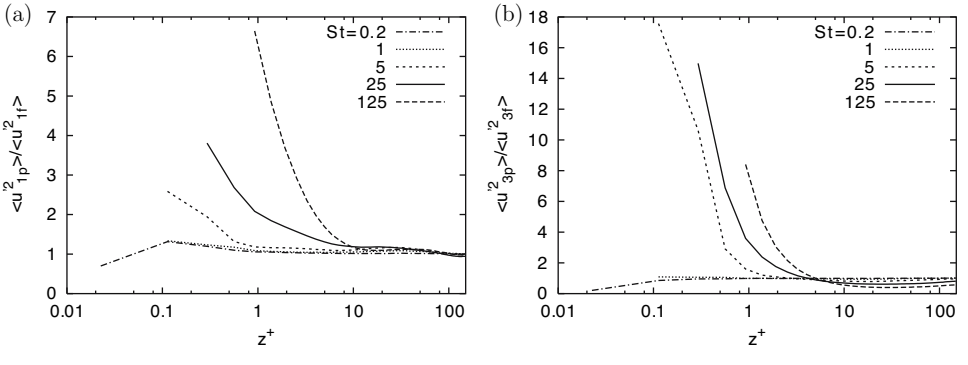

Figure 6. (a) Streamwise and (b) wall-normal particle-to-fluid Reynolds stresses, $\langle u'^2_{ip} \rangle / \langle u'^2_{if} \rangle$, as a function of the wall-normal coordinate, z^+.

particles ($St = 0.2$ and $St = 1.0$). For the $St = 5$ particles, Γ is still not very different from unity, except within 1 viscous unit from the wall, where it increases to a value of 2.5, roughly; for the larger particles ($St = 25$ and $St = 125$), Γ is $O(1)$ from the center of the channel up to roughly 10 viscous units from the wall. Approaching further the wall, Γ increases to values of about 4 for the $St = 25$ case and to values of about 7 for the $St = 125$ case. In the wall-normal direction (figure 6(b)), the near-wall changes are even more dramatic, particularly for the $St = 5$ particles. In this case, Γ increases by a factor of about 20, from $\Gamma \simeq 0.9$ at $z^+ \simeq 5$ to $\Gamma \simeq 18$ at $z^+ \simeq 0.1$.

Clearly, depending on the particle time scale considered, the reduction in the wall-normal fluid velocity fluctuation close to the wall may not be accompanied by an equivalent reduction in the wall-normal particle velocity fluctuation [12]. This tendency is quantified in figure 7, where the wall-normal behavior of the local equilibrium coefficient modeled using equation (4)

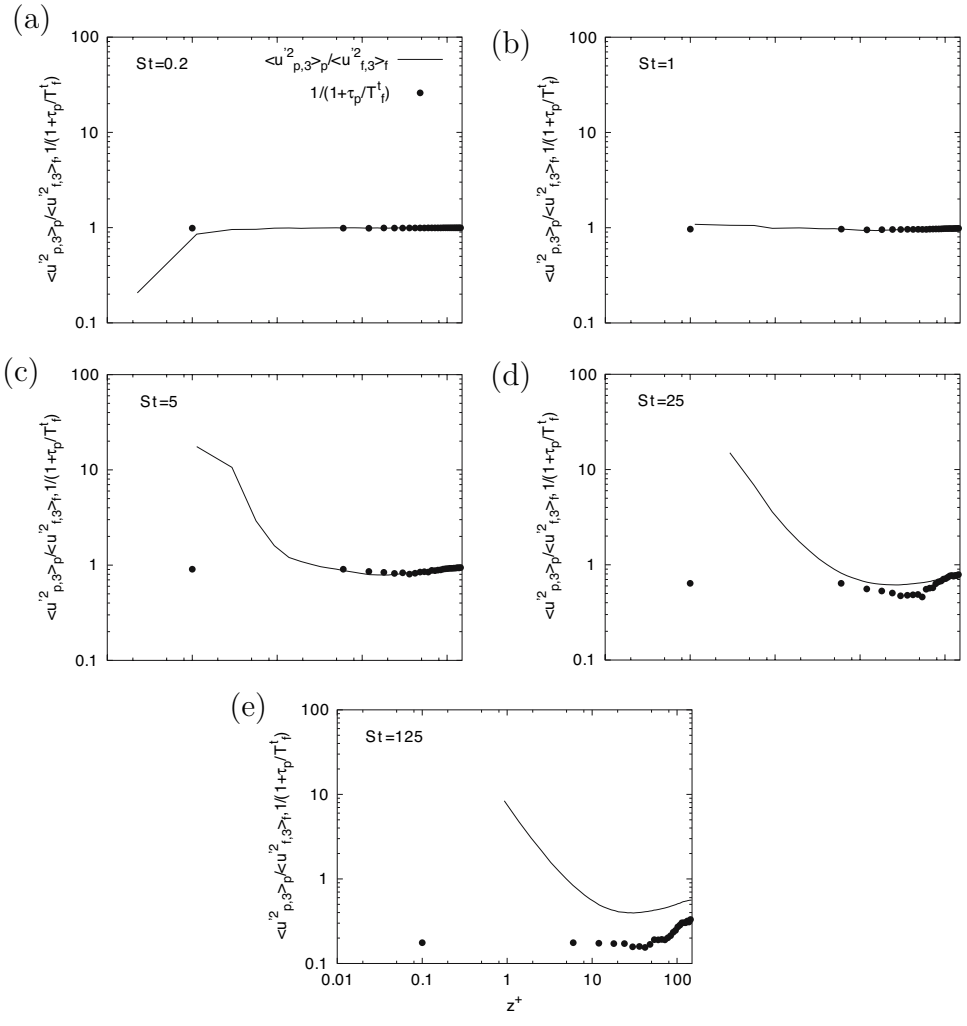

Figure 7. Comparison between the wall-normal particle-to-fluid Reynolds stress, $\langle u'^2_{p,3}\rangle / \langle u'^2_{f,3}\rangle$ (lines), and the local equilibrium coefficient Γ, modeled as $1/(1 + \tau_p / T_L^f)$ (symbols). (a) $St = 0.2$, (b) $St = 1$, (c) $St = 5$, (d) $St = 25$, and (e) $St = 125$ particles.

with $C = 1$ [7, 10] (symbols) is compared to the local equilibrium coefficient computed from the DNS dataset (solid line). The latter quantity is given by the wall-normal particle-to-fluid Reynolds stresses, $\langle u'^2_{p,3}\rangle_p / \langle u'^2_{f,3}\rangle_f$, as already shown in figure 6(b). All particle sets are considered.

Several conclusions can be drawn observing figure 7. First, regardless of the particle time scale, the value of Γ is roughly constant away from the wall ($z^+ > 5$ for $St = 5$ and $St = 25$); therefore, local-equilibrium models for particle deposition may give reasonable predictions. Second, the local equilibrium assumption works well even in the near-wall region if the particle time scale is sufficiently small ($St < 5$ or $\tau_p / T_L^f \ll 1$ in the present study). Third, for larger particle time scales ($St > 5$ or $\tau_p / T_L^f \sim O(1)$) the local-equilibrium assumption breaks down approaching the wall, where lines and symbols do not overlap anymore, and the reliability of predictions becomes questionable. Indeed, the assumption appears physically uncorrect everywhere in the $St = 125$ case (figure 7(e)). Similar issues have been previously discussed by Portela *et al.* [12], who studied numerically the near-wall behavior of particles in turbulent pipe flows. However, these authors presented results for rather large particle time scales ($St = 25$ and $St = 100$ based on the eddie turnover time, τ_f) and considered a situation of statistically steady particle concentration, which has not been achieved by our simulations.

4. Conclusions

In the present work, we have analyzed several Eulerian–Lagrangian statistics on the near-wall behavior of inertial particles in fully developed turbulent channel flow, considering a statistically developing condition for the particle concentration. The object of the analysis is to study the effect of using wall-dependent flow time scales to characterize particle dispersion in the turbulent wall layer. The Lagrangian integral time scale of the fluid, either seen by fluid tracers or seen by inertial particles, and the Kolmogorov time scale have been considered. Our results show that the Lagrangian integral time scale of the fluid is adequate to characterize particle wall deposition while the Kolmogorov time scale is not. Yet, when an integral time scale is used to model the local-equilibrium coefficient, problems may arise depending on the time scale of the particles. If the particle time scale is large (Stokes number larger than 5 in the present study), then the model of local equilibrium becomes inaccurate in the near-wall region; due to the turbophoretic effect, the reduction of the fluid velocity fluctuations, which decrease to zero at the wall, is not accompanied by an equivalent reduction of the particle velocity fluctuations along the wall-normal direction. From a practical perspective, this implies that simple local-equilibrium models, assuming a linear relation between the wall-normal Reynolds stresses of the particles and the fluid, are not able to give reasonable results very close to the wall. Present results are valid for low-Reynolds number turbulence; a Reynolds number dependence on Lagrangian correlations is possible and deserves further investigation. Another issue to be clarified is the effect of the concentration stage reached by the particles; a comparison of the current results with those obtained under statistically steady condition for the particle concentration will be made to quantify the effect of large integration time on particle statistics. From a qualitative viewpoint, we expect that the time scale variation seen by the particles will be maintained during the dispersion process.

References

[1] Young, B. and Hanratty, T.J., 1991, Trapping of solid particles at the wall in a turbulent flow. *AIChE Journal*, **37**, 1529–1536.

[2] Eaton, J.K. and Fessler, J.R., 1994, Preferential concentration of particles by turbulence. *International Journal of Multiphase Flow*, **20**, 169–201.
[3] Marchioli, C. and Soldati, A., 2002, Mechanisms for particle transfer and segregation in turbulent boundary layer. *Journal of Fluid Mechanics*, **468**, 283–315.
[4] Soldati, A., 2005, Particles turbulence interactions in boundary layers. *Zeitschrift für angewandte Mathematik und Mechanik,* **85**, 683–699.
[5] Picciotto, M., Marchioli, C. and Soldati, A., 2005, Characterization of near-wall accumulation regions for inertial particles in turbulent boundary layers. *Physics of Fluids,* **17**, 098101.
[6] Narayanan, C., Lakehal, D., Botto, L. and Soldati, A., 2003, Mechanisms of particle deposition in a fully-developed turbulent open channel flow. *Physics of Fluids,* **15**, 763–775.
[7] Young, J.B. and Leeming, A., 1997, A theory of particle deposition in turbulent pipe flow. *Journal of Fluid Mechanics,* **340**, 129–159.
[8] Cerbelli, S., Giusti, A. and Soldati, A., 2002, ADE approach to predicting dispersion of heavy particles in wall bounded turbulence. *International Journal of Multiphase Flow*, **27**, 1861–1879.
[9] Sergeev, Y.A., Johnson, R.S. and Swailes, D.C., 2002, Dilute suspension of high inertia particles in the turbulent flow near the wall. *Physics of Fluids,* A **14**, 1042–1055.
[10] Slater, S.A., Leeming, A.D. and Young, J.B., 2003, Particle deposition from two-dimensional turbulent gas flows. *International Journal of Multiphase Flow*, **51**, 275–283.
[11] van Haarlem, B., Boersma, B.J. and Nieuwstadt, F.T.M., 1998, Direct numerical simulation of particle deposition onto a free-slip and no-slip surface. *Physics of Fluids*, A **10**, 2608–2620.
[12] Portela, L.M., Cota, P. and Oliemans, R.V.A., 2002, Numerical study of the near-wall behaviour of particles in turbulent pipe flows. *Powder Technology*, **125**, 149–157.
[13] Lam, K. and Banerjee, S., 1992, On the condition of streak formation in bounded flows. *Physics of Fluids*, a **4**, 306–320.
[14] Soldati, A. and Banerjee, S., 1998, Turbulence modification by large organized electrohydrodynamic flows. *Physics of Fluids*, **10**, 1742–1756.
[15] Kuerten, J.G.M. and Vreman, A.W., 2005, Can turbophoresis be predicted by large-eddy simulation? *Physics of Fluids*, **17**, 011701.
[16] Iwamoto, K., Suzuki, Y. and Kasagi, N., 2002, Reynolds number effect on wall turbulence: toward effective feedback control. *International Journal of Heat Fluid Flow*, **23**, 678–689.
[17] Rouson, D.W. and Eaton, J.K., 2001, On the preferential concentration of solid particles in turbulent channel flow. *Journal of Fluid Mechanics*, **428**, 149–169.
[18] Maxey, M.R. and Riley, J.J., 1983, Equation of motion for a small rigid sphere in a nonuniform field. *Physics of Fluids*, **30**, 1915–1928.
[19] Chung, J.N. and Troutt, T.R. 1988, Simulation of particle dispersion in an axisymmetric jet. *Journal of Fluid Mechanics*, **186**, 199–222.
[20] Elghobashi, S. and Truesdell, G.C. 1992, Direct simulation of particle dispersion in a decaying isotropic turbulence. *Journal of Fluid Mechanics*, **242**, 655–700.
[21] Loth, E., 2000, Numerical approaches for motion of dispersed particles, droplets and bubbles. *Progress in Energy Combustion Science*, **26**, 161–223.
[22] Schiller, V.L. and Naumann, A., 1935, Über die grundlegenden Berechnungen bei der Schwerkraftaufbereitung. *Zeitschrift des Vereins Deutscher Ingenieure*, **77**, 318–320.
[23] Portela, L.M. and Oliemans, R.V.A. 2003, Eulerian–Lagrangian DNS/LES of particle–turbulence interactions in wall-bounded flows. *International Journal for Numerical Methods in Fluids*, **43**, 1045–1065.
[24] Wang, L.P. and Maxey, M.R. 1993, Settling velocity and concentration distribution of heavy particles in homogeneous isotropic turbulence. *Journal of Fluid Mechanics*, **256**, 27–68.
[25] Derevich, I.V. and Zaichik, L.I., 1988, Particle deposition from turbulent flow. *Fluid Dynamics*, **23**, 722–729.
[26] Kallio, G.A. and Reeks, M.W., 1989, A numerical simulation of particle deposition in turbulent boundary layer. *International Journal of Multiphase Flow*, **12**, 433–446.
[27] Simonin, O., Deutsch, E. and Minier, J.P. 1993, Eulerian prediction of the fluid/particle correlated motion in turbulent two-phase flows. *Applied Scientific Research*, **51**, 275–283.
[28] Reeks, M.W., 1983, The transport of discrete particles in inhomogeneous turbulence. *Journal Aerosol Science* **310**, 729–739.
[29] Deutsch, E. and Simonin, O., 1991. Large eddy simulation applied to the motion of particles in stationary homogeneous fluid turbulence. *Turbulence Modification in Multiphase Flows ASME FED*, **110**, 35–42.